Journal of Environmental Chemical Engineering

Gas phase hydrogenation of furfural to obtain valuable products using commercial Cr-free catalysts as an environmentally sustainable alternative to copper chromite

--Manuscript Draft--

Manuscript Number:	JECE-D-21-00254R1
Article Type:	Research Paper
Keywords:	Furfural; Hydrogenation; Cu/ZnO; furfuryl alcohol; 2-methylfuran
Corresponding Author:	Juan Antonio Cecilia, Ph.D. University of Málaga Málaga, SPAIN
First Author:	C.P. Jiménez-Gómez
Order of Authors:	C.P. Jiménez-Gómez
	Juan Antonio Cecilia, Ph.D.
	C. García-Sancho
	R. Moreno-Tost
	P. Maireles-Torres
Abstract:	Traditionally, copper chromite has been used in furfural hydrogenation to obtain valuable products, like furfuryl alcohol. However, the presence of Cr poses serious environmental issues, in such a way that different Cr-free catalysts has been proposed as alternative. In this work, two commercial Cu-based catalysts without Cr, currently used in alcohol reforming (R120) and water-gas shift (W220), have been successfully evaluated in FUR hydrogenation to produce selectively furfuryl alcohol. Both R120 and W220 catalysts were characterized, with special emphasis on the elucidation of metallic properties, dispersion and oxidation states of Cu species, and compared to copper chromite. The R120 catalyst attained the best catalytic performance and stability over time, reaching a turnover frequency (TOF) of 0.31 s -1 at 190 °C, after 1 h of reaction. The catalytic results reported that these Cr-free commercial catalysts have high potential to replace copper chromite as shown the stability test for 24h.

Graphical Abstract

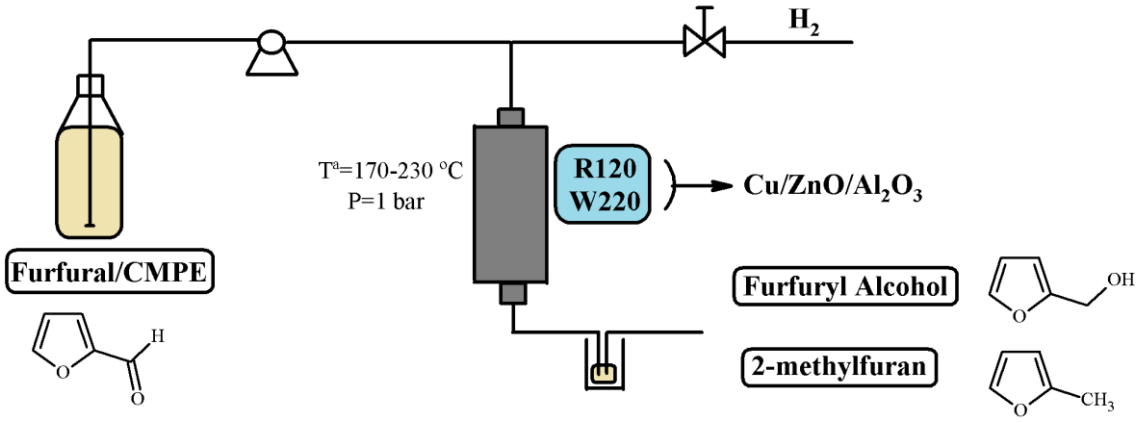

Highlights

Commercial Cr-free catalysts have shown excellent behavior in the furfural hydrogenation.

Strong interaction between Cu and ZnO particles leads to a higher activity and stability along the TOS.

ZnO has an electronic promoter effect on the Cu^0, while Al_2O_3 stabilizes the Cu particles.

The presence of Lewis acid sites (Cu^+) favors the formation of carbonaceous deposits.

Metal-sites are involved in the hydrogenation reaction, while acid sites influence in the hydrogenolysis reaction.

Scheme 1. Scheme of furfural hydrogenation.

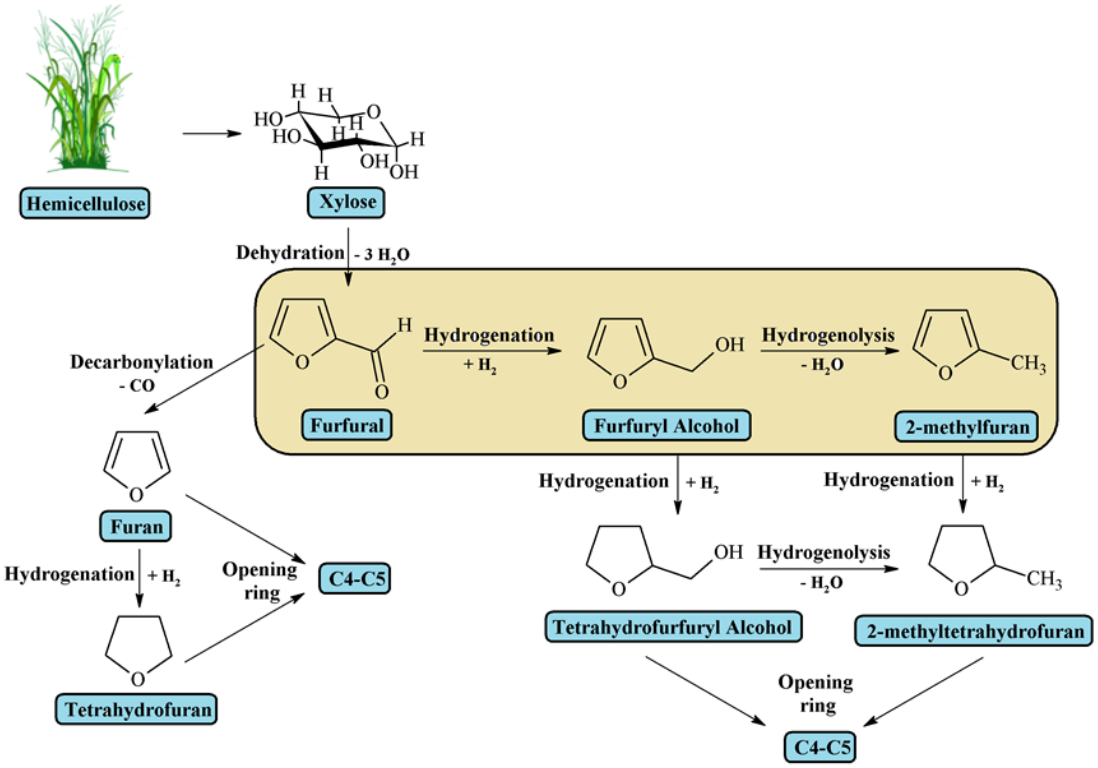

Scheme 2. Mechanism of the furfural hydrogenation.

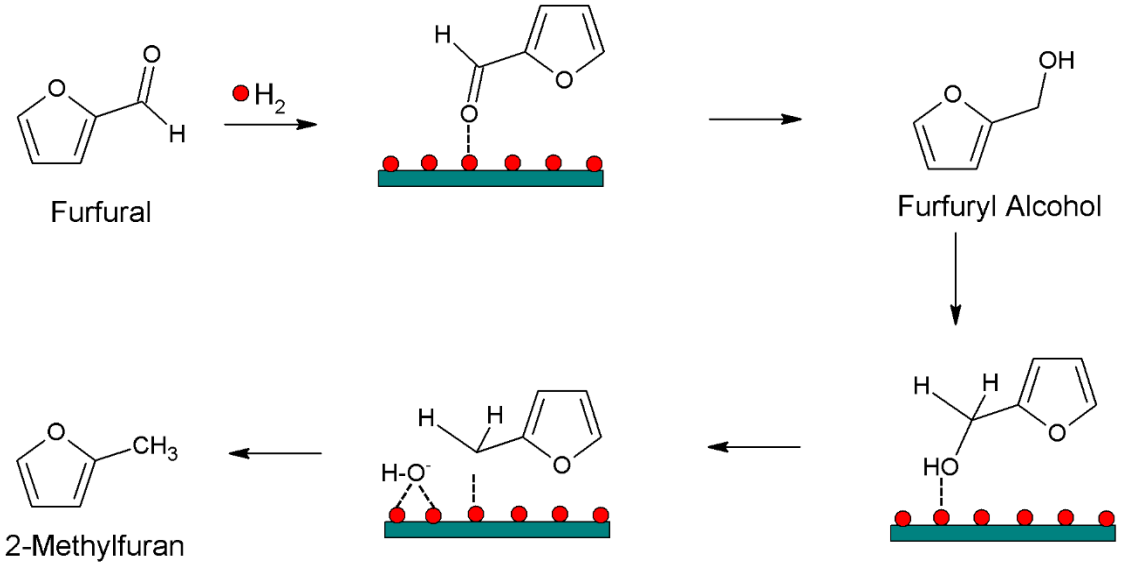

List of captions

Figure 1. H_2-TPR of commercial catalysts.

Figure 2. X-ray diffractograms of reduced catalysts and after 24 h of TOS. (Experimental conditions: 30 µmol active sites, temperature: 190 ºC, H_2 flow: 10 mL min^{-1}, feed flow: 2.3 $mmol_{FUR}$ h^{-1})

Figure 3. (A) Cu 2p core level and (B) Auger Cu_{LMM} spectra of reduced catalysts.

Figure 4. Catalytic performance of commercial catalysts at different reaction temperatures, as a function of time on stream (TOS). (Experimental conditions: 30 µmol active sites g^{-1}, H_2 flow: 10 mL min^{-1}, feed flow: 2.3 $mmol_{FUR}$ h^{-1}, H_2:FUR : 11.5 and WHSV: 1.5 h^{-1}).

Figure 5. MF yield using FUR or FOL in the feed after 1 h and 5 h of TOS for commercial catalysts. (Experimental conditions: 30 µmol active sites, temperature: 190 ºC, H_2 flow: 10 mL min^{-1}, feed flow: 2.3 $mmol_{FUR\ or\ FOL}$ h^{-1}, H_2:FUR : 11.5 and WHSV: 1.5 h^{-1})

Figure 6. FUR conversion (A), FOL yield (B) and MF yield (C) as a function of TOS over commercial catalysts. (Experimental conditions: 30 µmol active sites, temperature: 190 ºC, H_2 flow: 10 mL min^{-1}, feed flow: 2.3 $mmol_{FUR}$ h^{-1}, H_2:FUR : 11.5 and WHSV: 1.5 h^{-1})

Figure 7. (A) Cu 2p core level and (B) Auger Cu_{LMM} spectra of commercial catalysts after 24 h of TOS. (Experimental conditions: 30 µmol active sites, temperature: 190 ºC, H_2 flow: 10 mL min^{-1}, feed flow: 2.3 $mmol_{FUR}$ h^{-1}, H_2:FUR : 11.5 and WHSV: 1.5 h^{-1})

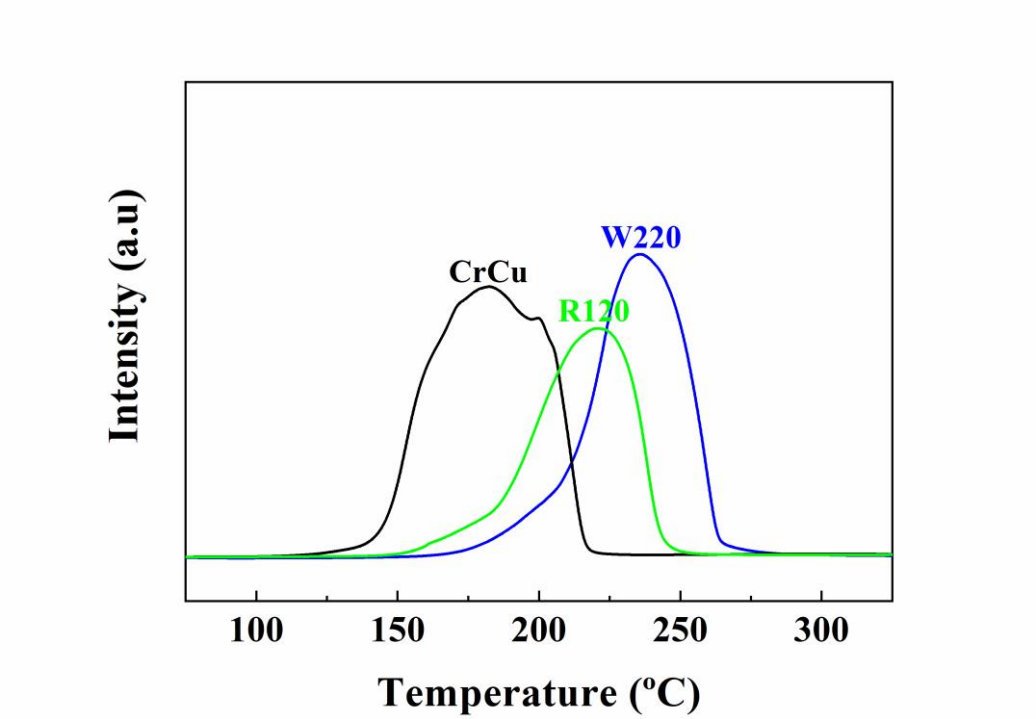
Intensity (a.u)
CrCu
W220
R120
100
150
200
250
300
Temperature (°C)

Figure 1

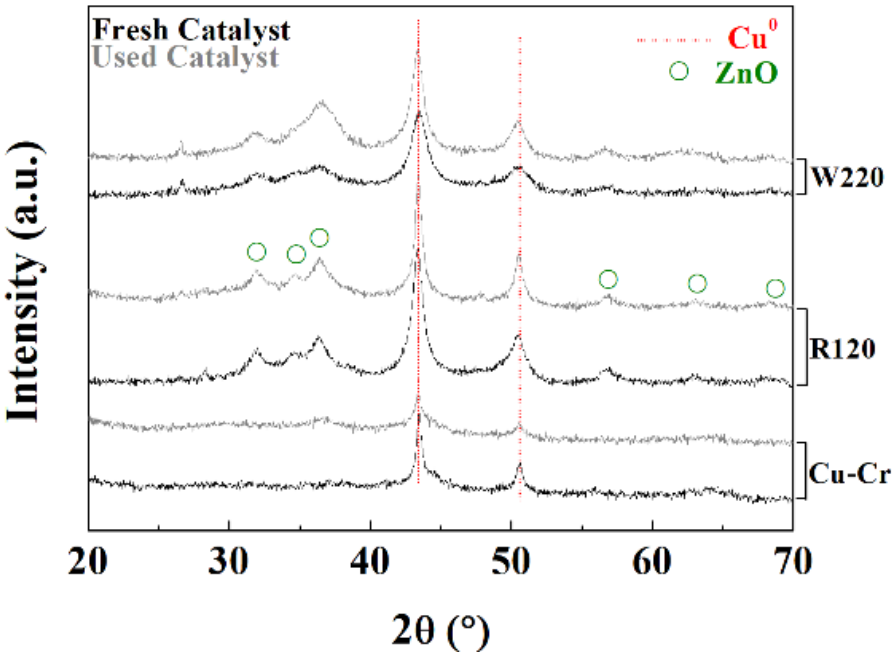
Fresh Catalyst
Used Catalyst
Cu0
ZnO
W220
R120
Cu-Cr
Intensity (a.u.)
20
30
40
50
60
70
2θ (°)

Figure 2

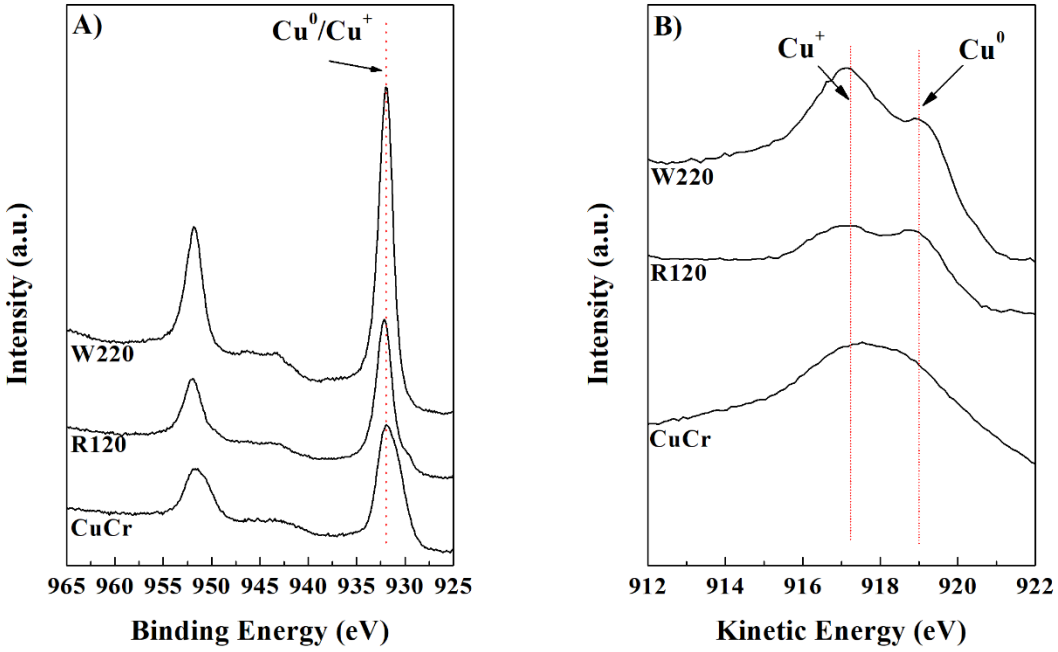
A)
Cu0/Cu+
W220
R120
CuCr
Intensity (a.u.)
965 960 955 950 945 940 935 930 925
Binding Energy (eV)
B)
Cu+
Cu0
W220
R120
CuCr
Intensity (a.u.)
912 914 916 918 920 922
Kinetic Energy (eV)

Figure 3

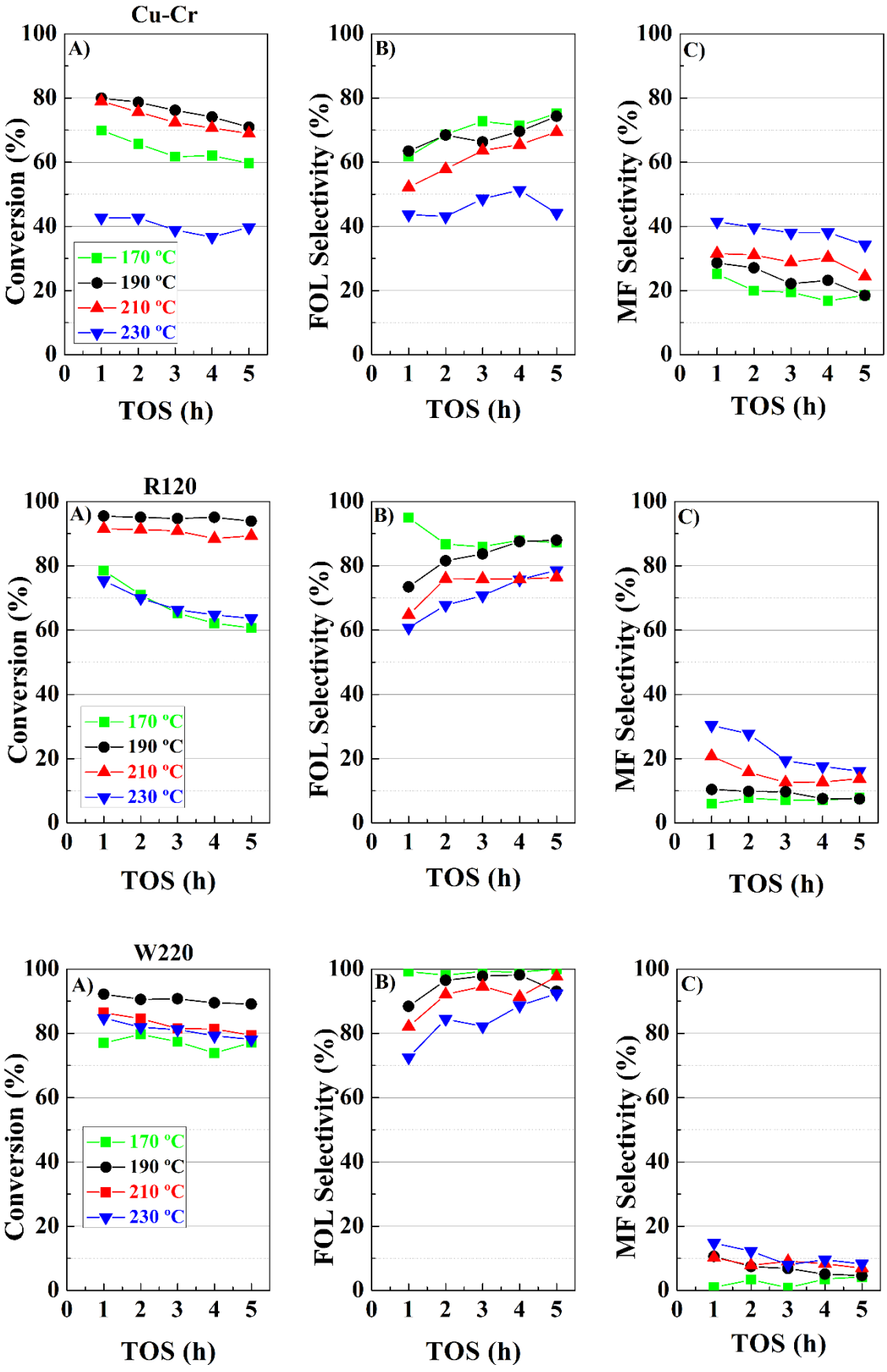
Cu-Cr
R120
W220
A)
B)
C)
Conversion (%)
FOL Selectivity (%)
MF Selectivity (%)
TOS (h)
170 °C
190 °C
210 °C
230 °C

Figure 4

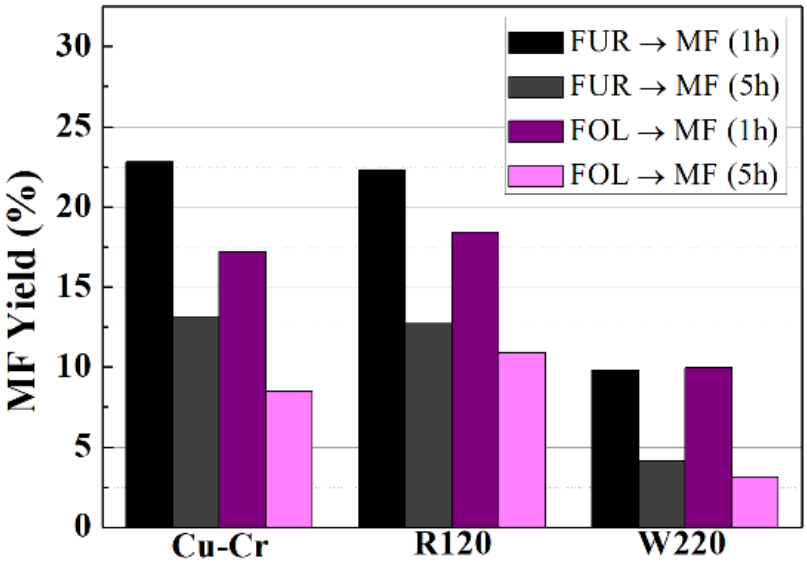
MF Yield (%)
30
25
20
15
10
5
0
Cu-Cr
R120
W220
FUR → MF (1h)
FUR → MF (5h)
FOL → MF (1h)
FOL → MF (5h)

Figure 5

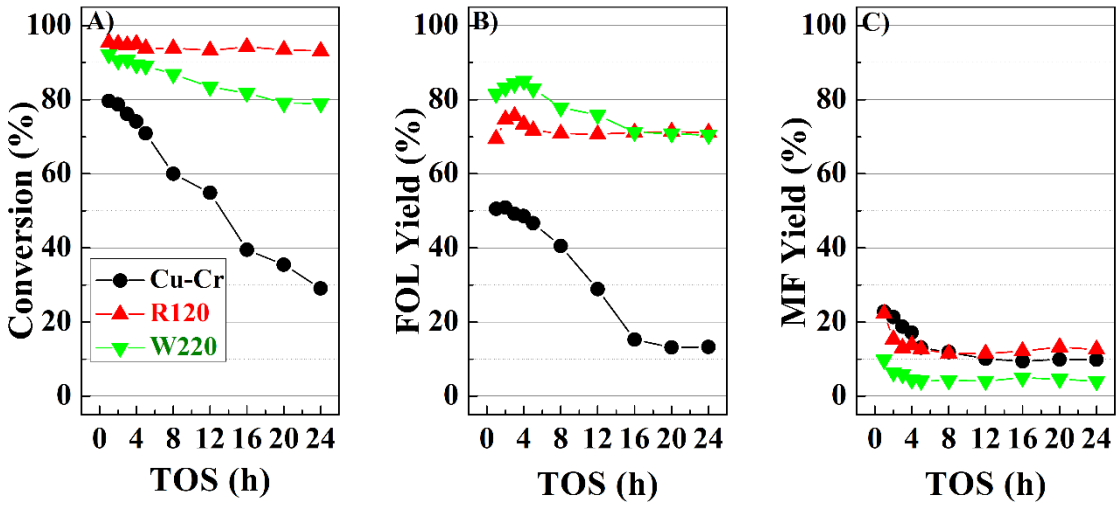
A)
B)
C)
Conversion (%)
FOL Yield (%)
MF Yield (%)
TOS (h)
Cu-Cr
R120
W220
0
20
40
60
80
100
0 4 8 12 16 20 24

Figure 6

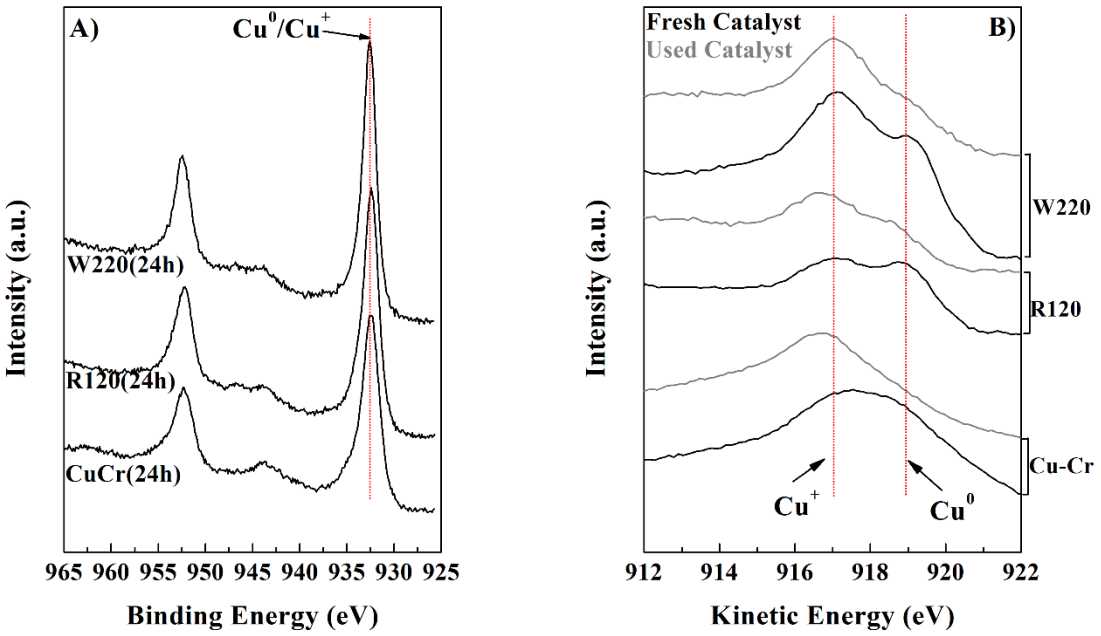
A)
Cu0/Cu+
W220(24h)
R120(24h)
CuCr(24h)
Intensity (a.u.)
965 960 955 950 945 940 935 930 925
Binding Energy (eV)
Fresh Catalyst
Used Catalyst
B)
W220
R120
Cu-Cr
Cu+
Cu0
Intensity (a.u.)
912 914 916 918 920 922
Kinetic Energy (eV)

Figure 7

Table 1. Atomic concentration data of catalyst precursors, fresh and spent catalysts, estimated by XPS analysis (In parentheses, bulk data obtained from XRF, balanced with oxygen).

	Atomic concentration (%) or atomic ratio									
Sample	**C**	**O**	**Cu**	**Cr**	**Al**	**Zn**	**Cu/Cr**	**Cu/Zn**	**Cu/Al**	**Cu/(Zn+Al)**
Catalyst Precursors										
Prec CuCr	18.8	51.6 (60.1)	13.7 (21.7)	16.4 (18.2)	-	-	0.84 (1.19)	-	-	-
Prec R120	31.0	29.4 (57.5)	7.6 (27.1)	-	27.6 (5.2)	5.0 (10.2)	-	1.52 (2.66)	0.28 (5.21)	0.23 (1.76)
Prec W220	36.3	33.9 (57.2)	8.4 (19.7)	-	33.3 (11.6)	7.9 (11.5)	-	1.06 (1.71)	0.25 (1.70)	0.20 (0.85)
Fresh Catalysts										
CuCr	29.1	39.3	6.7	25.0	-	-	0.27	-	-	-
R120	15.6	36.8	10.1	-	27.6	10.0	-	1.01	0.37	0.27
W220	22.7	26.1	11.0	-	33.6	7.0	-	1.57	0.33	0.27
Spent catalysts (after 24 h of TOS)										
s-CuCr	56.7	31.3	1.7	10.3	-	-	0.16	-	-	-
s-R120	38.7	31.1	2.7	-	19.9	6.9	-	0.39	0.14	0.10
s-W220	54.2	23.2	2.1	-	17.5	3.1	-	0.68	0.12	0.10

Table 2. Textural and acid/base properties of the reduced catalysts.

Sample	S_{BET} ($m^2\ g^{-1}$)	Pore volume ($cm^3\ g^{-1}$)	Average pore size (nm)	Acid sites ($\mu mol\ g^{-1}$)	Basic sites ($\mu mol\ g^{-1}$)
CuCr	55	0.128	16.7	264	15
R120	93	0.224	10.2	78	29
W220	103	0.194	7.0	65	41

Table 3. Dispersion, Cu particle size and metallic surface of the reduced commercial catalysts (estimated by N_2O titration, XRD and CO isotherms).

Sample	Dispersion[a] (%)	Particle size (nm)			Metallic surface[a]		S_{Cu^+}[b]
		N_2O	XRD	CO	($m^2_{Cu}\ g_{Cu}^{-1}$)	($m^2_{Cu}\ g_{cat}^{-1}$)	($m^2\ g^{--1}$)
CuCr	27.0	3.7	20.0	44.4	174.1	85.6	1.8
R120	5.6	18.8	12.5	37.9	35.8	16.4	0.5
W220	4.7	22.3	9.3	38.3	30.2	22.4	2.3

[a] Determined by N_2O titration
[b] Surface area of Cu^+ estimated from the irreversible CO isotherms

Gas phase hydrogenation of furfural to obtain valuable products using commercial Cr-free catalysts as an environmentally sustainable alternative to copper chromite

C.P. Jiménez-Gómez, J.A. Cecilia*, C. García-Sancho, R. Moreno-Tost, P. Maireles-Torres

Universidad de Málaga, Departamento de Química Inorgánica, Cristalografía y Mineralogía (Unidad asociada al ICP-CSIC), Facultad de Ciencias, Campus de Teatinos, 29071 Málaga (Spain).

E-mail: jacecilia@uma.es

Abstract

Traditionally, copper chromite has been used in furfural hydrogenation to obtain valuable products, like furfuryl alcohol. However, the presence of Cr poses serious environmental issues, in such a way that different Cr-free catalysts has been proposed as alternative. In this work, two commercial Cu-based catalysts without Cr, currently used in alcohol reforming (R120) and water-gas shift (W220), have been successfully evaluated in FUR hydrogenation to produce selectively furfuryl alcohol. Both R120 and W220 catalysts were characterized, with special emphasis on the elucidation of metallic properties, dispersion and oxidation states of Cu species, and compared to copper chromite. The R120 catalyst attained the best catalytic performance and stability over time, reaching a turnover frequency (TOF) of 0.31 s^{-1} at 190 °C, after 1 h of reaction. The catalytic results reported that these Cr-free commercial catalysts have high potential to replace copper chromite as shown the stability test for 24h.

Keywords: Furfural; hydrogenation; $Cu/ZnO/Al_2O_3$; furfuryl alcohol; 2-methylfuran

1. Introduction

Currently, bioethanol and furfural are the two main products obtained from the sugar platform with an annual production of 280000 metric tons. Furfural has attracted the interest of both academic and industrial research groups, since it is considered a versatile molecule for the synthesis of a wide variety of high value-added chemicals [1,2]. This is because the furfural molecule is highly reactive, that is, prone to experience a diversity of reactions. Considering only hydrogenation processes, furfural (FUR) can be transformed into valuable products, such as furfuryl alcohol (FOL), tetrahydrofurfuryl alcohol (THFOL), 2-methylfuran (2-MF), 2-methyltetrahydrofuran (2-MTHF), furan, tetrahydrofuran, or even aliphatic alcohols [3] (Scheme 1). These catalytic processes can be performed in both vapor and liquid phase, requiring hydrogenation catalysts [4–7]. The gas-phase hydrogenation of FUR is the preferred industrial process for FOL production. However, this has some drawbacks associated to the high reaction temperature, as well as the use of non-environmentally friendly catalysts (chromium chromite in industrial hydrogenation of furfural). Moreover, in most cases, metal-based catalysts are prone to deactivation. Nevertheless, the liquid-phase batchwise operation process is less suitable for large-scale applications, because the expensive equipment required for working at high pressure and temperature conditions, and the time delay between successive batch reactions.

On the other hand, the reduction of FUR can take place through direct hydrogenation on metal-based catalysts, by interaction of its carbonyl group or furan ring with metal sites [8] or through catalytic transfer hydrogenation (CTH), where an alcohol acts as H-donor to reduce the carbonyl group of an aldehyde or ketone by a six-membered intermediate [9].

Among metal active phases, Cu is preferred if both furfuryl alcohol or 2-methylfuran are considered the target hydrogenated products [8,10–16], due to its ability to hydrogenate the carbonyl group, or selectively break the C-O bond, without affecting furan ring or C-C bonds. This selectivity is being used to produce bio-renewable chemicals or biofuels from biomass, thus allowing the upgrading of compounds derived from lignocellulosic carbohydrates, such as furfural and 5-hydroxymethylfurfural.

Nowadays, the commercial catalyst used for the reduction of FUR to FOL is copper chromite [17–19], which is not environmentally friendly because of the concerns related to chromium species, or safe disposal of the spent catalyst.

In general, the catalytic hydrogenation of furfural yields FOL as main product and 2-MF as by-product. Moreover, the formation of 2-MF, resulting from the hydrogenolysis of the C-O bond of FOL [10,19], is favored with the reaction temperature [10,20,21]. There is a general agreement that the maximum yield of FOL depends on the metallic surface area of copper particles [22,23]. Dong *et al.* [21] found a relationship between 2-MF yield and the acidity of Cu/SiO_2 catalysts, being promoted the FOL hydrogenolysis by superficial Cu^+ species. Yang *et al.* [23] showed that the modulation of the interaction between Cu particles and ZnO affected the catalytic performance, being favored the C-O cleavage for catalysts with a high concentration of strong acid sites, whereas a high dispersion of copper improved the selectivity towards FOL. However, Deutsh *et al.* [24] did not observe a clear correlation between the amount of acid sites and superficial Cu^+ species, as they could not relate the hydrogenolysis of the C-O bond of 5-methylfurfuryl alcohol with the presence of Cu^+ in copper chromite catalysts.

Rao *et al*. [25] also studied the hydrogenation of FUR with copper chromite, concluding that Cu^+ should play a key role, being necessary the presence of both Cu^+ and Cu^0 for

attaining the maximum activity. This fact was corroborated by these authors in the study of catalysts based on metallic Cu deposited on different types of carbonaceous supports [26], as they observed that the TOF (intrinsic activity) decreased when the Cu^0 content increased. In both types of catalysts, the activation of hydrogen took place on the metallic copper surface. Nagaraja *et al.* [11] also showed the necessary presence of Cu^+, when copper was supported on MgO, to reach the highest furfural conversion. On the other hand, Liu *et al.* [19], by means of XAFS and AES analyses, demonstrated that Cu^0 was the unique active species in copper chromite, being irrelevant the presence of oxidized copper species for explaining the catalytic behavior. In general it has been reported that weakly acidic (SiO_2) [14,27], amphoteric (ZnO, CeO_2) [12,13] or basic (MgO) [11] supports weaken this interaction in comparison with strong acid supports, which are more susceptible to deactivation. The use of catalysts with lower acidity leads to more labile interaction, so the desorption of FUR and/or the obtained products is more favorable. In this way, several author have pointed out that Cu^0 sites are involved in the homolytic cleavage of hydrogen molecules, favoring the adsorption of FUR by the carbonyl group to form FOL [16], while hydrogenolysis of FOL to MF usually requires a small amount of acid sites [21].

Considering that Cu-based catalysts are highly selective to high value-added chemicals, such as FOL and 2-MF [3], the present research envisions to evaluate the catalytic activity in the hydrogenation of FUR of two commercial Cu/ZnO-Al_2O_3 catalysts used for the methanol synthesis and hydrogen production. One of the roles ascribed to ZnO and Al_2O_3 is to act as physical spacer, thus improving the copper dispersion during the catalyst synthesis [28,29]. Moreover, the sintering resistance of Cu and ZnO nanoparticles can also be ascribed to the strong Cu-ZnO interaction, which would limit the growth of Cu^0 crystallites. That could mean that the intimate contact between copper

and ZnO particles generates an interface where zinc could be partially reduced and copper partially oxidized [30]. In this sense, previous authors have reported that the strong interactions Cu-ZnO generate an interface were Zn^{2+} can be partially reduced and Cu^0 partially oxidized improving the catalytic behavior [29,31]. This data could confirm the formation of a solid solution of Cu^+ in the lattice of ZnO (wurtzite) during the reduction treatment [32–34], which can provide interstitial cations, or oxygen vacancies [35,36]. On the other hand, the solubility is limited by the required electroneutrality. The charge deficiency can also be compensated by the presence of trivalent cations, like Al^{3+} [34].

Other authors have pointed out that Cu^+ and ZnO can form a partial solid solution [30,32,37]. In addition, Al^{3+} species can also have a beneficial effect on the catalytic activity [36], since these species contribute to facilitate the reducibility of ZnO, increasing the number of O vacancies. The partial reduction of Cu, leads to hydrogenation sites Cu^0 and Lewis acid sites (Cu^+), which plays an important role and many hydrogenation reaction such as furfural [11,12], dimethyl malonate [38], citral [39], crotonaldehyde [40] and dimethyl oxalate[41–43].

The study of superficial composition and its influence on the catalytic performance, in terms of furfural conversion and selectivity towards FOL and 2-MF, and catalyst stability, as well, was studied. Bearing in mind that the commercial catalyst for FOL production is copper chromite, this will also be evaluated for comparison purposes. Finally, this research puts special emphasis on the optimization of catalytic parameters to minimize deactivation, which is an important drawback in the gas-phase FUR hydrogenation, mainly due to copper sintering, the oxidation of the active phase and the formation of carbonaceous deposits [14,19,25].

2. Materials and methods

2.1. Reagents.

Commercial copper chromite ($CuCr_2O_4$·. CuO) was supplied by Aldrich, methanol reforming (HiFUEL® R120) and low temperature water gas shift (HiFUEL® W220) copper-based catalysts were purchased from Alfa Aesar. Chemicals employed in furfural hydrogenation were furfural (Sigma-Aldrich, 99%), cyclopentyl methyl ether (Sigma-Aldrich, 99.9%) as solvent, and o-xylene (Sigma- Aldrich, 99.9%) as internal standard. The gases were He (Air Liquide 99.99%), H_2 (Air Liquide 99.999%), N_2 (Air Liquide 99.9999%), He/N_2O (5% vol. in N_2O, Air Liquide 99.99%) and H_2/Ar (10% vol. in H_2, Air Liquide 99.99%).

2.2. Characterization of catalysts

Powder X-ray diffraction (XRD) patterns were obtained in a PAN analytical X´Pert Pro automated diffractometer, in Bragg–Brentano reflection configuration, by using a Ge (111) primary monochromator (Cu $K\alpha_1$) and the X´Celerator detector with a step size of 0.017° (2θ), between 10° and 70° in 2θ with an equivalent counting time of 712 s $step^{-1}$. The crystallite size (D) was calculated by using the Williamson-Hall equation [44], $B \cos \theta = (K \lambda/D) + (2 \varepsilon \sin \theta)$, where θ is the Bragg angle, B is the full width at half maximum (FWHM) of the XRD peaks, K is the Scherrer constant, λ is the wavelength of the X ray and ε the lattice strain [44].

Elemental bulk composition was determined by X-Ray Fluorescence with wavelength disperse X-ray fluorescence spectrometer (ARL ADVANTXP) and a UNIQUANT software. The X-ray tube was set at 60 kV.

Hydrogen temperature-programmed reduction (H_2-TPR) experiments were carried out by using 0.08 g of catalyst precursor, previously treated with a He flow (35 mL min^{-1}) at 100 °C for 30 min. After cooling to room temperature, the H_2 consumption was monitored between 50 and 350 °C, by using an Ar/H_2 flow (48 mL min^{-1}, 10 vol.% H_2)

with a heating rate of 10 °C min^{-1}. Water formed in the reduction process was trapped by passing the outcoming flow through a cold finger, immersed into a solid N_2-liquid/isopropanol bath (-80 °C). The H_2 quantification was performed with an on-line Thermal Conductivity Detector (TCD).

Metal surface area and dispersion were evaluated by N_2O titration, by using 0.080 g of catalyst [12,13]. This method is based on the formation of a monolayer of Cu_2O by oxidation of superficial Cu^0 with a N_2O flow, according to the reaction: $2Cu^0 + N_2O \rightarrow Cu_2O + N_2$. Before analysis, the CuO phase is reduced under a 10 vol.% H_2/Ar flow (48 mL min^{-1}) and a rate of 5 ºC min^{-1} during 1 h. Then, samples were purged under a He flow and cooled down to 60 ºC. The oxidation of Cu^0 to Cu^+ is carried out by chemisorption of N_2O (5 vol.% N_2O/He) at 60 ºC during 1 h. Later, the catalyst was again purged with a He flow and cooled to room temperature. After this, the reduction of Cu_2O to Cu(0) was done by raising the temperature under a 10 vol.% H_2/Ar flow (48 mL min^{-1}).

Textural parameters were evaluated from N_2 adsorption-desorption isotherms at -196 °C (automatic ASAP 2020 Micromeritics apparatus). Prior to measurements, samples were outgassed at 200 °C and 10^{-4} mbar overnight. Specific surface areas (S_{BET}) were determined by using the Brunauer–Emmett–Teller (BET) equation considering a nitrogen molecule cross section of 16.2 $Å^2$. Density functional theory (DFT) was used to deduce pore size distribution plots.

The basicity of catalysts was studied by temperature-programmed desorption of CO_2, where approximately 0.1 g of sample was pretreated under a helium flow (60 mL min^{-1}) at 500 ºC for 30 min (heating rate of 10 ºC min^{-1}). The reaction temperature was lowered to 80 ºC and a pure CO_2 stream (60 mL min^{-1}) was subsequently introduced into the reactor for 30 min. The CO_2-TPD was conducted between 100 and 800 ºC

under a He flow (10 ºC min^{-1} and 30 mL min^{-1}) and the amount of CO_2 evolved was analyzed using a thermal conductivity detector. The water formed in the reduction reaction was trapped by passing the exit flow through a cold finger immersed in ice-salt. The amount of acid sites was determined by temperature-programmed desorption of ammonia (NH_3-TPD). 0.08 g of catalyst was previously pre-treated under a He flow (40 mL min^{-1}) from room temperature to 550 °C, with a heating rate of 10 °C min^{-1}, and then was cooled using the same gas until 100 °C. After that, the catalyst was saturated with NH_3 for 5 min. Then, a He flow (40 mL min^{-1}) was passed to eliminate the physisorbed ammonia. Finally, temperature-programmed desorption was carried out by heating the samples from 100 to 550 °C, at a heating rate of 10 °C min^{-1}. The desorbed ammonia was quantified by a thermal conductivity detector (TCD).

The X-ray photoelectron spectra were obtained with a Physical Electronics PHI 5700 spectrometer with non-monochromatic Mg K_α radiation (300 W, 15 kV, 1253.6 eV) with a multichannel detector. The spectra were recorded in the constant-pass energy mode at 29.35 eV with a 720 μm diameter analysis area. Charge referencing was measured against adventitious carbon (C 1s at BE: 284.8 eV). The PHI ACCESS ESCA-V6.0 F software package was used for the acquisition and data analysis. A Shirley-type background was subtracted from the signals. All of the recorded spectra were fitted with Gaussian-Lorentzian curves to determine more accurately the binding energies of the different element core levels. All samples were stored in sealed vials with an inert solvent to avoid oxidation. The samples were prepared in a dry box under a N_2 flow and analyzed directly without previous treatment, and the solvent was evaporated before the introduction of samples into the analysis chamber.

2.3. Catalytic tests

The vapor phase hydrogenation of FUR was carried out at atmospheric pressure in a ¼'' quartz reactor. For each experiment, an amount of catalyst equivalent to 30 μmol of Cu active sites, as determined by N_2O, was pelletized with a sieve range between 325-400 μm, so the quantities of 0.0286 mg of CuCr, 0.1500 mg of Prec R120 and 0.1091 mg of Prec W220 were mixed with silicon carbide (SiC) and loaded in the reactor to obtain a catalytic bed of 1.5 cm of length. Each sample was placed in the middle of the reactor between two layers of glass beads and quartz wool. Prior to the catalytic tests, catalysts were reduced *in-situ* according to their H_2-TPR profiles, using a H_2 flow of 60 mL min^{-1} for 1 h to ensure a total reduction of Cu^{2+}. Then, catalysts were cooled down to the selected reaction temperature. Once this temperature was reached, a flow (3.87 mL h^{-1}) of a FUR solution in CPME (5 vol.%), to prevent blockage of reactor lines, was injected continuously with a Gilson 307SC piston pump (model 10SC) to obtain a WHSV of 1.5 h^{-1} (referred to FUR fed) using a H_2 flow in the range of 10-60 mL min^{-1} as carrier gas. CPME was selected as solvent due to it is considered an environmental friendly solvent, which is employed in several biomass valorization processes, like the selective dehydration of lignocellulosic pentoses to FUR [45].

The stability of the cyclopentyl methyl ether (CPME) was evaluated under similar catalytic conditions to those used in the gas-phase furfural hydrogenation, confirming that CPME was inert regardless the catalyst used.

Both furfural and reaction products were analyzed using a Shimadzu GC-14A gas chromatograph equipped with a flame ionization detector and a CP-Wax 52CB capillary column. The furfural conversion and selectivity were calculated and defined as follows:

$$\text{Conversion (\%)} = \frac{\text{mol of furfural converted}}{\text{mol of furfural fed}} \times 100$$

$$\text{Selectivity}\ (\%) = \frac{\text{mol of the product}}{\text{mol of the furfural converted}} \times 100$$

FUR, FOL and MF were calibrated using commercial reagents. The non-detected products were determined from:

$$\text{N. D.}_{products} = \left(\text{FUR}_{fed}\right) - \left(\text{FUR}_{non\ converted} + \text{FOL}_{obtained} + \text{MF}_{obtained}\right)$$

Considering that mass transfer limitations can occur, the Weisz-Prater criterion (C_{WP}) was applied to determine if diffusion in the pores is limiting the reaction. Internal mass transfer can be neglected if the C_{WP} is lower than 0.3. This analysis has been performed for all the experiments, and the parameters used are summarized in the Supplementary Information. The C_{WP} values are in all cases lower than 0.3, so the mass transfer limitations can be ruled out under the reaction conditions tested and, therefore, the catalysts are working under kinetic regime.

3. Results and Discussion

The bulk and surface atomic concentrations of catalyst precursors (before reduction) have been determined by X-ray fluorescence (XRF) and X-ray photoelectron spectroscopy (XPS), respectively (**Table 1**). Copper chromite displays the highest surface Cu content (13.7 at%), while R120 and W220 present close values, 8.4 and 7.6 at%, respectively. However, the bulk and surface compositions are quite different, although copper is the main element contributing to the bulk composition for the three precursors. It is striking that XPS data revealed a higher Al content for R120 and W220 than those obtained by XRF, which would suggest a high proportion of aluminum on the catalyst surface.

As regards the XRD study, broad diffraction peaks point out low crystallinity or small crystallite sizes in all precursors (**Fig. S1**). Prec R120 and Prec W220 show similar

diffraction patterns, with peaks at 2θ (º)= 32.3, 35.7, 38.9, 58.2 and 61.5, which can be ascribed to a tenorite CuO phase (ICDD: 00-041-0254), whereas those at 2θ (º)= 31.7, 47.5, 56.7, 66.2 and 68.1 correspond to the hexagonal wurtzite ZnO structure (ICDD: 04-007-1614). Moreover, the broadening of peaks resulted in overlapping, thus rendering difficult the assignation to a particular crystalline CuO and ZnO phase. Finally, a diffraction peak attributed to a γ–AlOOH phase (ICDD: 01-074-2901) can also be observed at 2θ (º)= 14.5 for Prec R120 and Prec W220. The diffractogram of Prec CuCr exhibits peaks at 2θ (º)= 30.4, 35.5, 37.2, 38.7, 43.1, 57.2 and 63.3, characteristic of copper chromite, $CuCr_2O_4$ (ICDD: 00-034-0424). Taking into account that pure copper chromite contains a bulk Cu^{2+}:Cr^{3+} molar ratio of 1:2, XRF data would point out that commercial Prec CuCr is not a pure phase, consisting of CuO·and $CuCr_2O_4$, since the Cu:Cr molar ratio is close to 1:1. However, the diffraction signals of CuO are indistinguishable due to broad and intense peaks of copper chromite, and, accordingly, it should be as well dispersed nanoparticles in copper chromite.

H_2-TPR profiles reveal that copper chromite is more easily reducible, being copper species completely reduced at 225 ºC, while R120 and W220 require reduction temperatures of 250 and 275 ºC, respectively (**Fig. 1**). These temperatures were selected to reduce catalyst precursors, and for ensuring the total reduction of active phase, precursors were maintained at the reduction temperature for 1 h. The H_2 consumption starts at lower temperature for copper chromite than for Cr-free catalysts, which can be explained by a combination of two factors: a stronger interaction between CuO particles and ZnO-Al_2O_3 phases [39,46] and the presence of smaller particles in the case of copper chromite, even undetected by XRD. The higher reduction temperature needed for Prec W220 could be due to its higher surface concentration of aluminum, since the effect of aluminum species on CuO reduction has been reported by several research

groups. Thus, Yang *et al.* [22] observed that aluminum species can overcoated the interface of CuO/ZnO, raising the reduction temperature of CuO/ZnO-Al_2O_3 catalysts. However, Hu *et al.* [47] concluded that Al_2O_3 can retard the reduction of Cu^{2+} to Cu^0, due to the stabilization of Cu^+ phases.

The reduction of the Cr-free precursors led to the formation of metallic copper nanoparticles, being the unique crystalline phase, along with ZnO, detected by XRD (**Fig. 2**). Thus, the diffraction peaks at 2θ (º) = 43.4 and 50.5 were ascribed to metallic copper, Cu^0 (ICDD: 04-0836), and those at 2θ (º) = 31.8, 34.7, 36.4, 56.9, 63.0 and 68.0 to hexagonal wurtzite ZnO crystallites (ICDD: 01-070-2551). It is striking that diffraction peaks assigned to Al species were not observed in reduced catalysts. After reduction of Prec CuCr, diffraction peaks of the copper chromite phase disappear and new peaks appear at 2θ (º) = 43.6 and 50.7, due to metallic copper (PDF 01-077-3038), and the presence of cuprous chromite ($CuCrO_2$) is also detected at 2θ (º) = 36.5 and 62.4 (PDF 00-39-0247), although the intensity of these peaks was very low and noisy [24,31,48,49]. Cr-free catalysts showed smaller Cu crystallite sizes (12.5 and 9.3 nm for R120 and W220, respectively), similar to that observed for ZnO nanoparticles (11.1 and 6.7 nm, respectively). Nevertheless, for CuCr, Cu crystallites were bigger (20 nm), although the presence of smaller nanoparticles could be inferred by H_2–TPR. In any case, it is noteworthy that, after reduction, despite the high copper loadings, metallic copper is highly dispersed as nanoparticles smaller than 20 nm.

To evaluate the surface chemical composition of catalysts, XPS data were acquired. The Cu 2p core level spectra of all catalysts (**Fig. 3A**) display a similar profile, with a band at ~932 eV in the Cu $2p_{3/2}$ region, which is assigned to reduced Cu species [50]. The absence of the shake-up satellite of Cu^{2+}would confirm its absence. However, from the Cu 2p core level spectra, it is not possible to discern between both reduced Cu species

($Cu^{0/+}$), and the Auger Cu_{LMM} line must be analyzed to determine their contribution (**Fig. 3B**) [12,14], considering that the kinetic energy of their corresponding Auger electrons differs by about 2 eV [24]. In all cases, the coexistence of both reduced copper species was detected, which would indicate the partial reduction of Cu^{2+} species on the catalyst surface. These data do not totally agree with those inferred from H_2-TPR, where the reduction of Cu^{2+} species seemed to be almost total. Nevertheless, the partial superficial oxidation of Cu^0 to Cu^+ could be ascribed to sample handling before XPS analysis. The presence of Cu^+ species can also be attributed to the incorporation of a small fraction of Cu species within the ZnO structure, thus rendering Cu species less reducible. In the same way, the presence of Cu^+ species in CuCr catalyst could be ascribed to the formation of a $CuCrO_2$ phase, although this phase was hardly detected in the corresponding XRD pattern (**Fig. 2**).

The deconvolution of Auger Cu_{LMM} bands reveals that Cu^0 (**Table S1**) is the main contribution for R120 (peak at ca. 919 eV), whereas the CuCr and W220 catalysts showed a major contribution of partially reduced Cu^+ species.

Concerning XPS data of Zn for R120, Zn $2p_{3/2}$ core level spectra, the Auger Zn_{LMN} band and modified Auger parameter would confirm the absence of modifications during the reduction process, being Zn^{2+} present in all cases (**Table S1**) [51]. Therefore, there are no spectroscopic evidences for the partial reduction of Zn^{2+}, as set down by other authors [52,53]. In the case of W220, the Zn 2p peak shifts by 0.8 eV toward lower BE after reduction, which could be explained by the existence of electron-rich Zn^{2+} cations, as for example in a $Zn^{\delta+}$ state, where δ is lower than 2, as was reported by other authors previously [31]. These data agree with its higher reduction temperature observed in the H_2-TPR study (**Fig. 1**). It has been previously demonstrated that the coexistence of

ZnO_x layers and Cu^+ in catalysts can play an important role in methanol synthesis [54–56].

Regarding the O 1s core level, it can be deconvoluted into two bands, ascribed to hydroxyl (higher BE) and oxidic (lower BE) species. The contribution at higher BE shows a marked decrease after reduction, being more noticeable for CuCr (**Table S1**). In the case of Cr-free catalysts, the decrease in the hydroxyl band is lesser pronounced, which would suggest some modification of the electronic interaction in the Cu-ZnO interface, as was reported by other authors [23,57].

Concerning atomic concentration values, CuCr suffers a diminution of the Cu/Cr atomic ratio after reduction, thus revealing a superficial Cr-enrichment. However, the Cu/Zn atomic ratio for the Cr-free catalysts were not varied significantly (**Table 1**).

Textural properties were estimated by N_2 adsorption-desorption at -196 ºC (**Fig. S2**). According to the IUPAC classification, the isotherm of CuCr can be classified as Type II, typical of non-porous or macroporous solids, while those of R120 and, mainly, W220 catalysts resemble to that of mesoporous solids (Type IVa) [58]. The CuCr catalyst displays a Type H3 loop, which is associated to non-rigid aggregates of plate-like particles, or macropores that are not completely filled with pore condensate, as inferred from the N_2 adsorption increase at high relative pressures [58]. The hysteresis loops of R120 and W220 are Type H2b, ascribed to structures with partially or totally closed pores [58]. The specific surface area (S_{BET}), reported in **Table 2**, indicates that CuCr is the catalyst with the lowest S_{BET}, only 55 m^2g^{-1}, while R120 and W220 display higher values (93 and 103 m^2 g^{-1}, respectively). Regarding pore volume, the CuCr catalyst again displays the lowest value (0.128 cm^3 g^{-1}), while R120 and W220 catalysts have 0.224 and 0.194 cm^3 g^{-1}, respectively. Likely, Al species with a small particle size can

also contribute to the specific surface area of Cr-free catalysts, improving their textural properties.

The pore size distribution profiles, determined by the DFT method (Fig. 2SB) [59], show a heterogeneous range of pore sizes for the CuCr catalyst, being the catalyst with the highest proportion of macropores. In the case of R120 catalyst, the pore size distribution is more homogeneous, being in the range of 1-50 nm, while the W220 catalyst exhibits the narrowest pore width distribution (1-30 nm).

From these textural data, it can be concluded that porosity could be mainly attributed to interparticle voids, since larger particles, as deduced from XRD in the case of the CuCr catalyst (**Fig. 2**), led to lower surface area and pore volume. On the contrary, the smaller crystallite sizes of R120 and W220 lead to improved textural properties (**Table 2**).

The acidity was evaluated from temperature-programmed desorption of ammonia (**Fig. S3A** and **Table 2**). Despite Cr-free catalysts possess higher surface area and pore volume, these catalysts display a low concentration of acid sites (78 and 65 μmol g^{-1} for R120 and W220, respectively), which are weak according to their low desorption temperatures. This low acidity is ascribed to the amphoteric behavior of ZnO and γ–AlOOH, which, in turn, has an acidity lower than that shown by Al_2O_3. In the case of the CuCr catalyst, the amount of acid sites is considerably higher (264 μmol g^{-1}), which should be attributed to the presence of $CuCrO_2$ or Cr_2O_3, as shown by XRD and XPS, in which the Cu^+ and Cr^{3+} may act as a Lewis acid sites, increasing the acidity. In this sense, the Auger LMM lines revealed that W220 catalyst also displays a high proportion of Cu^+ species (**Fig. 3**), although the NH_3-TPD reported low acidity in the same range of R120 catalyst. Thus, Cr^{3+} species should exhibit a higher Lewis acidity than Cu^+ ones.

The concentration of basic sites was evaluated by CO_2-TPD (**Fig. S3B**). These catalysts display a low amount of basic sites, although the Cr-free catalysts present higher values also due to their amphoteric character [60] (**Table 2**). In the case of CuCr, the number of basic sites is much lower due to $CuCrO_2$ or Cr_2O_3 hardly display basic character.

N_2O titration is a well-known methodology to determine the amount of surface metallic sites (Cu^0) [23,61,62], while the irreversible CO adsorption isotherm provides a measurement of Cu^+ ions and the total CO uptake could be considered approximately the surface concentration of copper in all oxidation states [40,63].

CuCr catalyst displays the highest dispersion of Cu^0 species (27%), the highest metallic surface area and the lowest metal crystallite sizes. As it was mentioned, the Prec CuCr catalyst showed segregated CuO particles that were not detected by XRD analysis, which would imply the existence of an amorphous state or tiny particles. Moreover, H_2-TPR analysis demonstrated that Cu^{2+} species were more easily reduced, which was ascribed to both copper in copper chromite and small CuO nanoparticles. Therefore, these results seem reasonable, though they might disagree with XRD data, but it should be noticed that XRD analysis provides average values based on the peak width at half height. Nevertheless, both CO isotherm and N_2O titration allow to obtain average values of Cu^+ and Cu^0 particle sizes, so it seems logical that different results may appear. The high reducibility and small crystallite size of Cu particles in the CuCr catalyst could cause an over-oxidation in the N_2O oxidation step. From this fact, it can be expected a higher metallic surface and a smaller particle size in comparison to data obtained from XRD using the Williamson-Hall equation.

For R120 catalyst, the particle size determined by XRD and N_2O are roughly similar, considering experimental errors of both analytical methods. In contrast, the W220 catalyst shows larger particle sizes from N_2O titration than by XRD, which should

imply a lower copper dispersion. In this sense, XPS analysis reported that W220 catalyst, after reduction, exhibits an interface with intimate contact between Cu and ZnO particles, leading to the formation of interfacial $Zn^{\delta+}$ and Cu^{+} species. Cu^{+} is not able to react with N_2O, i.e. the consumption of N_2O is lower than expected. Moreover, as Cu^{+} species are stabilized by ZnO [32], even preventing its reduction, the second reduction step of surface Cu^{+} leads to a lower hydrogen consumption, and, consequently, underestimates the values for W220 by N_2O titration.

However, considering data obtained from total CO adsorption, similar results can be found for the three catalysts, in terms of particle size and metal dispersion (**Table 3**). The surface area associated to Cu^{+} obtained from the irreversible CO isotherms could be due to Cu^{+} in cuprous chromite, detected by XRD, and the presence of Cu^{+} in Cr-free catalysts detected by Auger analysis. In this case, although both Cr-free catalysts showed higher CO adsorption, which is agreement with the higher concentration of Cu^{+} species detected by XPS analysis (**Table 1**).

The analysis of the cell parameters for ZnO, Prec R120 and Prec W220 shows modification of the cell parameters (**Table S3**). Considering that Cu^{2+} in a tetrahedral environment (0.57 Å) is slightly smaller than Zn^{2+} (0.60 Å), the partial substitution could cause a contraction of the lattice parameter and hence to a decrease in the *c* parameter [35,64], mainly in the case of Prec W220. The stronger interaction of the Cu^{2+} species located inside wurtzite structure would lead to its partial reduction. These data are in agreement with the CO irreversible adsorption, where a clear interaction between Cu^{+} species and CO could be inferred, since Cu^{2+} species were not detected from XPS and Cu^{0} species do not interact with CO molecules. In the case of Prec R120, the lattice parameters are closer to the wurtzite structure. This implies that the inclusion

of Cu^{2+} species into the ZnO structure is less favorable, in such a way that the reducibility of Cu^{2+} species is easier, leading to a higher proportion of metal Cu species.

4. Catalytic tests

The experimental conditions (temperature, H_2 flow, H_2:FUR molar ratio or WHSV) were selected according to previous research, being the optimal conditions to reach the maximum conversion and yield values [12,14]. Concerning to the commercial catalysts reported in the present study, it can be observed how these catalysts are very active in gas-phase hydrogenation of furfural, in the temperature range of 170-230ºC (**Fig. 4**). The Cr-free catalysts attained the highest catalytic performance between 190-210 ºC, whereas the decline of furfural conversion with time-on-stream (TOS) depended on both the nature of catalyst and reaction temperature. In this sense, it is noteworthy that R120 hardly suffered deactivation, with a FUR conversion of 95% after 5 h of TOS, at 190 ºC. The deactivation of Cu-based catalysts is a well-known drawback of gas-phase FUR hydrogenation, already reported in the case of CuCr [19,25] and $Cu/ZnO/Al_2O_3$ [22] catalysts. A higher reaction temperature (230°C) did not improve FUR conversion, because FUR is prone to polymerize, causing a blockage of active sites involved in FUR hydrogenation [12,19]. Catalyst deactivation can also be due to the strong interaction of FUR and/or FOL with the active phase, hindering the access of new FUR molecules to be reduced [10,14]. The physico-chemical characterization of catalysts has demonstrated both the low acidity of R120 and W220, with a small concentration of acid sites, which seem to provide them a higher stability along TOS.

The turnover frequency (TOF), a measure of the catalytic activity per active site, i.e. intrinsic reactivity of a catalyst [65], was calculated from the equation:

$$TOF\ (s^{-1}) = -\frac{F/W}{M}\ x\ \ln\ (1 - X)$$

where F is the molar rate of furfural (mol s^{-1}), W is the catalyst weight (g), M is the number of the loaded active sites calculated from N_2O titration (mol g^{-1}) and X is the conversion of furfural. However, FUR conversions were close to 100% and therefore far from differential conditions, so an integral analysis was used [66]. This equation assumes a pseudo first-order, which could be justified by the large excess of hydrogen and that the active phase is superficial Cu^0. The profiles of TOF data at 190 ºC as a function of TOS (**Fig. S4**) would point out that this might be influenced by the adsorption of products on active sites, thus diminishing those available for another catalytic cycle, mainly when the catalyst works at high furfural conversion. Thus, it is observed that TOF reaches its highest value for R120.

Considering that the reactivity studies have been carried out loading the same number of active sites (30 μmol), the activity cannot only be explained in terms of metallic Cu^0 surface area. In the case of CuCr, the XPS analysis have shown that the reduction treatment provoked a superficial enrichment in chromium and, furthermore, the Cu^+/Cu^0 ratio was above unity in CuCr, in the same range to those found for Cr-free catalysts (**Table S2**), confirming the presence of $CuCrO_2$ in CuCr. Therefore, this phase, formed as the expense of copper chromite, $CuCr_2O_4$, should be partially covering Cu^0 particles, thus decreasing the number of active sites, demonstrating that chromium species are not active in this reaction, as Liu *et al.* previously pointed out [19]. Thus, the role of cuprous chromite in the catalytic performance should be less beneficial than the presence of ZnO and/or Al_2O_3 for Cr-free catalysts since the incorporation of Cu favors the formation of slightly reduced Zn species ($Zn^{\delta+}$) and O vacancies, which can provide adsorbed hydrogen to copper nanoparticles [33,51,67].

The analysis of selectivity patterns has revealed that an increase in the reaction temperature causes a progressive rise of the MF selectivity, in agreement with previous

works pointing out that hydrogenolysis of FOL to MF is favored at higher temperature [8,19]. However, CuCr was not so selective towards either reaction product (**Fig. 4**), although the hydrogenation of FUR to FOL was favored, obtaining a selectivity about 70% after 5 h of TOS, at temperatures between 170 and 210 ºC. At the highest reaction temperature (230ºC), FOL and MF yields were very similar (between 40-45%), since the formation of MF is favored [8], which is also prompted by the presence of acid sites in CuCr (**Table 2**). On the other hand, both R120 and W220 catalysts were more selective to FOL. It is also noticeable that R120 is slightly more selective to MF than W220, mainly at higher temperatures, in spite of both catalysts are based on a $Cu/ZnO/Al_2O_3$ phase. From the catalytic data, it can be inferred the great potential of these Cr-free commercial catalysts, employed in other catalytic processes such as methanol reforming and water gas shift, in furfural hydrogenation, achieving higher FOL yields in comparison to copper chromite, which is the commercial catalyst employed in the gas-phase furfural hydrogenation.

Although the beneficial interaction (electronic, SMSI effect) between Cu^0 and metal oxides has been largely demonstrated in several catalytic processes, the role of Cu^+ is still debatable in hydrogenation processes. In this sense, it has been proposed a synergistic effect between Cu^0 and Cu^+, being the former responsible of H_2 dissociation, whereas Cu^+ interacts with the C=O bond of reactants, as was indicated in the CO chemisorption, acting as an electrophilic center [43,68]. In the case of furfural hydrogenation, Nagaraja *et al.* [11] proposed the necessity of both Cu^0 and Cu^+ species for attaining an optimal performance, although they did not indicate which was such optimal ratio. Rao *et al.* [26] affirmed that Cu^+ was involved in the catalytic process and TOF decreased as the $Cu^0/(Cu^0+Cu^+)$ ratio approached unity. By means of *operando* EXAFS studies, Zhang *et al.* [69] demonstrated that copper chromite can be stabilized

by a thin layer of alumina, and Cu^{+} was reduced to Cu^{0} under reaction conditions, and both species appeared as active phases, though a low Cu^{+} concentration reduced the furfural hydrogenation activity. On the other hand, Liu *et al.* [19] discarded the participation of Cu^{+} species in the catalytic activity, and metallic copper was the only species involved as active site, whereas Liu *et al.* [70] attributed the high performance of a Cu/MgO catalyst to the synergistic effect between Cu^{0} and Lewis basic sites, without the involvement of Cu^{+}. These results reflect that such influence, synergism or cooperation depends on the catalyst studied, and it is not possible to depict a unique image of the catalytic process. Concerning the catalysts tested in the present work, the role of Cu^{+} remains ambiguous and not clear due to oxidation state of Cu species can evolve along the reaction, since Cu^{+} species can be reduced in the reaction medium, while Cu^{0} species can be oxidized by the presence of H_2O generated as by-product in the hydrogenolysis reaction of FOL to MF (**Table S1** and **Table S2**). In addition, it is expected that other parameters, such as the acidity can also affect to the catalytic behavior, so both Cu^{+} and Cu^{0} species must change along the reaction.

On the other hand, the effect of feeding FUR or FOL on the MF formation was evaluated (**Fig. 5**). The use of FOL in the feed does not improve the selectivity towards MF, obtaining values relatively close to those reached when FUR was fed. This fact implies that the reaction follows the following route FUR → FOL → MF. The discrepancy between the MF yields depending on the feed may be due to the different enthalpy of adsorption of FUR and FOL on the catalyst surface [10]. According to the proposed Langmuir-Hinshelwood mechanism [71], after adsorption of FOL on the catalyst surface, it is reduced with the H_2 activated on Cu^{0} sites, so these data point out that the adsorption of FOL should be more energetically favored on CuCr and R120 catalysts than on W220. It is noticeable that the catalytic performance of R120

resembles more that of CuCr than that of W220, although R120 and W220 possess a similar chemical composition and totally differ from CuCr. Despite the similar behavior in terms of 2-MF yield, R120 and CuCr have important differences in terms of surface Cu^+ content. If these Cu^+ species were involved in MF production, the highest yield would be attained for CuCr. However, this trend is not observed for all catalysts, since W220 catalyst, with a high concentration of surface Cu^+ sites (**Table S2**), displays a poor 2-MF yield, with a very similar behavior regardless of the feed used. From the obtained data, it can be inferred that the hydrogenolysis reaction of C-OH bond is directly related to the amount of acid sites [21,23], where acidity of CuCr is three times higher than that of Cr-free catalysts. Therefore, it is expected that Cu^0 should be involved in the hydrogenation reaction of the carbonyl group of FUR but rather these sites must be involved in the activation of H_2 and in the adsorption of FUR, as shown by the mechanism proposed by Rao *et al.* [25] and Sitthisa *et al.* [10]. These authors indicate that the hydrogenolysis of the C-OH groups may be due to the presence of active sites with a high hydrogenation capacity. In the case of the W220 catalyst, the presence of active sites with lower hydrogenating capacity, like Cu, and the low proportion of acid sites makes this catalyst to have a lower hydrogenolysis activity than those existing in R120 and mainly CuCr (**Fig. 4**). Similar results came from Deutsch *et al.* [24], who studied the activity of copper chromite in the hydrogenolysis of 5-methylfurfuryl alcohol, observing a linear relationship between catalytic activity and density of Cu^0 sites. In the case of the Cu^+ sites, from CO chemisorption data, it could be inferred that these are dissolved in the ZnO structure, which could chemisorb FUR molecules through the carbonyl group (on-top adsorption), activating it for its subsequent hydrogenation to FOL.

In the next study, a long-term stability test was carried out during 24 h of TOS at 190ºC (**Fig. 6**). The catalytic results show that CuCr undergoes a progressive deactivation, reaching a FUR conversion of only 29%, after 24 of TOS. This deactivation could be ascribed to its highest acidity and high proportion of Cu^{+} species, which strongly interact with FUR and/or FOL molecules. In the case of the Cr-free catalysts, these are more resistant to deactivation, maintaining conversion values of 93 and 79% for R120 and W220, respectively. The lower deactivation could be due to their lower amount of acid sites. Thus, the higher acidity of CuCr, with a high proportion of strong acid sites (roughly 60%), can play a detrimental effect on the catalyst stability due to the progressive coverage of active sites by carbonaceous deposits due to their strong interaction of FUR and/or FOL, as was previously demonstrated from TPO experiments [13]. Regarding FOL and MF yields (**Fig. 6B-C**), both gradually decrease for CuCr along the TOS, with values of 13 and 9%, respectively, after 24 h. However, the two Cr-free catalysts showed a steady selectivity towards FOL, leading to a yield of 70% after 24 h of TOS. However, the MF yield suffers a fast decrease in the first hours of TOS, confirming that these catalysts are more prone to suffer deactivation by the formation of carbonaceous deposits. After the first hours, MF yield remains below 13% in both cases. On the other hand, the catalytic results suggest that the hydrogenation sites only involved in the FUR→FOL process seem to be less prone to deactivate, which could be inferred from the stable FOL yield and the concomitant decrease in the MF yield after the first hours of reaction.

In order to elucidate the modifications that the catalysts undergo throughout the furfural hydrogenation after 24 h of reaction at 190ºC, they were recovered and stored in an inert solvent, to prevent oxidation, and analyzed by XRD and XPS. X-ray diffraction patterns of spent catalysts (**Fig. 2**) are similar to those of fresh ones, discarding the formation of

new crystalline phases. In this sense, the low selectivity towards MF could limit the formation of water as by-product, which could oxidize Cu^0 to form Cu_2O crystals. However, these new diffraction peaks were not observed. The analysis of Cu crystallite sizes by the Williamson-Hall method reveals that the spent CuCr catalyst preserves the size (around 20 nm). This is in agreement with data reported by Lui *et al.* [19], who showed that Cu particle size of copper chromite did not significantly increase, even at temperatures above 300ºC. The crystallite size of the W220 catalyst raises slightly from 9.3 to 11.8 nm, while the growth is more pronounced for R120 (from 12.5 to 18.5 nm), which could be explained by the stronger interaction between Cu and ZnO in W220, minimizing sintering. In any case, this loss of active sites by sintering would be limited, since a high catalytic stability is maintained over R120 and W220 catalysts, so the deactivation by sintering could be discarded in all catalysts.

The composition of the spent catalyst surface was studied by XPS (**Fig. 7**). In all cases, the Cu 2p core level spectra evidences a unique contribution at 932.5 eV, which together with the absence of the typical shake-up satellite of Cu^{2+} species, would discard the existence of divalent copper presence. Moreover, in all cases, a detailed analysis of Auger Cu_{LMM} spectra shows an increase in the Cu^+ contribution (at 917 eV), as the higher Cu^+/Cu^0 ratio demonstrates (**Table S4**). Those Cu^+ species were not detected by XRD (**Fig. 2**), so the oxidation must occur on the catalyst surface, leading to low crystallinity phases, whose formation could be favored by H_2O generated in the hydrogenolysis process. The increase in the amount of Cu^+ species can favor the strong interaction with FUR and FOL, leading to the formation of carbonaceous deposits on active sites (**Table 1**). In the case of CuCr, a marked decrease in the superficial Cr content is observed, so Cr^{3+} acid sites clearly contribute to the deactivation process. Despite Cr content decreases on the surface of CuCr, the Cu/Cr molar ratio was lower

after the catalytic test, suggesting that carbonaceous species are preferentially deposited on surface copper sites. Concerning R120 and W220 catalysts, the decrease in surface Cu concentration is quite similar, 61 and 57% of the initial amount, respectively. However, R120 maintained FUR conversion for 24 h, whereas it was partially reduced for W220. Cu/Zn and Cu/Al molar ratios (**Table 1**) display a clear decrease after the catalytic process. However, the Al/Zn molar ratio slightly increases after the reaction, which could indicate that regions of intimate contact between Cu and ZnO are more prone to the deposition of carbonaceous species, but also confirming that these sites would be the most active, although they are deactivated more quickly. The Auger Cu_{LMM} study reveals that R120 displays the highest concentration of metal Cu^0 sites, being the most active and stable catalyst. A higher proportion of Cu^0 sites seems to difficult the formation of carbonaceous deposits, as indicated the XPS data (**Table 1**), resulting in a longer catalyst life. In this way, it can be concluded that R120 catalyst would present the best structure-activity relationship, in which a high proportion of metal Cu^0 species are well-dispersed on ZnO and Al_2O_3 leading to a catalyst with lower proportion of acid sites, thus avoiding its deactivation.

Conclusions

Commercial $Cu/ZnO/Al_2O_3$ catalysts are more active and stable than copper chromite in gas-phase FUR hydrogenation, being very selective to FOL. However, it does not exit a clear relationship between metallic surface area and catalytic activity, i.e., the most active catalyst does not possess the highest metallic surface area, as determined from N_2O titration, probably due to a possible over-oxidation of the reduced copper chromite (CuCr) with N_2O. An intimate and strong interaction between Cu and ZnO particles leads to a higher activity and stability over time. Al_2O_3 and, mainly, ZnO could play an important role in the activation of Cu sites, thus avoiding metal particles sintering. Cu^+

sites can also chemisorb FUR molecules through the carbonyl group, but, in the case of CuCr, these Cu^+ sites seem to have a lower ability to activate this carbonyl group. In fact, Cu^+ sites could serve as electrophilic centers, where FUR and/or FOL can be adsorbed leading to the generation of carbonaceous deposits, which can block the active sites along the TOS, being the main reason of the catalyst deactivation.

Acknowledgments

The authors are grateful to financial support from the Spanish Ministry of Innovation, Science and Universities (Project RTI2018-094918-B-C44) and FEDER (European Union) funds. J.A.C. and C.G.S. thank University of Malaga for contracts of PhD incorporation. R.M.T. thanks to the Spanish Ministry of Economy and Competitiveness (IEDI-2016-00743) for the financial support within the I3 program.

References

[1] K.J. Zeitsch, The Chemistry and Technology of Furfural and its Many By-Products, Elsevier, Amsterdam, 2000.

[2] B. Kamm, P.R. Gruber, M. Kamm, Biorefineries-Industrial Processes and Products: Status Quo and Future Directions, Wiley-VCH, 2008. https://doi.org/10.1002/9783527619849.

[3] K. Yan, G. Wu, T. Lafleur, C. Jarvis, Production, properties and catalytic hydrogenation of furfural to fuel additives and value-added chemicals, Renew. Sustain. Energy Rev. 38 (2014) 663–676. https://doi.org/10.1016/j.rser.2014.07.003.

[4] Y. Wang, P. Prinsen, K.S. Triantafyllidis, S.A. Karakoulia, A. Yepez, C. Len, R. Luque, Batch versus Continuous Flow Performance of Supported Mono- and Bimetallic Nickel Catalysts for Catalytic Transfer Hydrogenation of Furfural in Isopropanol, ChemCatChem. 10 (2018) 3459–3468.

https://doi.org/10.1002/cctc.201800530.

[5] Y. Wang, P. Prinsen, K.S. Triantafyllidis, S.A. Karakoulia, P.N. Trikalitis, A. Yepez, C. Len, R. Luque, Comparative Study of Supported Monometallic Catalysts in the Liquid-Phase Hydrogenation of Furfural: Batch Versus Continuous Flow, ACS Sustain. Chem. Eng. 6 (2018) 9831–9844. https://doi.org/10.1021/acssuschemeng.8b00984.

[6] Y. Wang, D. Zhao, D. Rodríguez-Padrón, C. Len, Recent advances in catalytic hydrogenation of furfural, Catalysts. 9 (2019). https://doi.org/10.3390/catal9100796.

[7] M. Audemar, Y. Wang, D. Zhao, S. Royer, F. Jérôme, C. Len, K. De Oliveira Vigier, Synthesis of furfuryl alcohol from furfural: A comparison between batch and continuous flow reactors, Energies. 13 (2020) 1–10. https://doi.org/10.3390/en13041002.

[8] S. Sitthisa, D.E. Resasco, Hydrodeoxygenation of furfural over supported metal catalysts: A comparative study of Cu, Pd and Ni, Catal. Letters. 141 (2011) 784–791. https://doi.org/10.1007/s10562-011-0581-7.

[9] M.J. Gilkey, B. Xu, Heterogeneous Catalytic Transfer Hydrogenation as an Effective Pathway in Biomass Upgrading, ACS Catal. 6 (2016) 1420–1436. https://doi.org/10.1021/acscatal.5b02171.

[10] S. Sitthisa, T. Sooknoi, Y.G. Ma, P.B. Balbuena, D.E. Resasco, Kinetics and mechanism of hydrogenation of furfural on Cu/SiO_2 catalysts, J. Catal. 277 (2011) 1–13. https://doi.org/10.1016/j.jcat.2010.10.005.

[11] B.M. Nagaraja, A.H. Padmasri, B. David Raju, K.S. Rama Rao, Vapor phase selective hydrogenation of furfural to furfuryl alcohol over Cu-MgO coprecipitated catalysts, J. Mol. Catal. A Chem. 265 (2007) 90–97.

https://doi.org/10.1016/j.molcata.2006.09.037.

[12] C.P. Jiménez-Gómez, J.A. Cecilia, D. Durán-Martín, R. Moreno-Tost, J. Santamaría-González, J. Mérida-Robles, R. Mariscal, P. Maireles-Torres, Gas-phase hydrogenation of furfural to furfuryl alcohol over Cu/ZnO catalysts, J. Catal. 336 (2016) 107–115. https://doi.org/10.1016/j.jcat.2016.01.012.

[13] C.P. Jiménez-Gómez, J.A. Cecilia, I. Márquez-Rodríguez, R. Moreno-Tost, J. Santamaría-González, J. Mérida-Robles, P. Maireles-Torres, Gas-phase hydrogenation of furfural over Cu/CeO_2 catalysts, Catal. Today. 279 (2017) 327–338. https://doi.org/10.1016/j.cattod.2016.02.014.

[14] C.P. Jiménez-Gómez, J.A. Cecilia, R. Moreno-Tost, P. Maireles-Torres, Selective Production of 2-Methylfuran by Gas-Phase Hydrogenation of Furfural on Copper Incorporated by Complexation in Mesoporous Silica Catalysts, ChemSusChem. 10 (2017) 1448–1459. https://doi.org/10.1002/cssc.201700086.

[15] C.P. Jiménez-Gómez, J.A. Cecilia, R. Moreno-Tost, P. Maireles-Torres, Selective Furfural Hydrogenation to Furfuryl Alcohol Using Cu-Based Catalysts Supported on Clay Minerals, Top. Catal. 60 (2017) 1040–1053. https://doi.org/10.1007/s11244-017-0804-2.

[16] Y. Shi, Y. Zhu, Y. Yang, Y.-W.Y.W. Li, H. Jiao, Exploring Furfural Catalytic Conversion on Cu(111) from Computation, ACS Catal. 5 (2015) 4020–4032. https://doi.org/10.1021/acscatal.5b00303.

[17] L.W. Burnett, I.B. Johns, R.F. Holdren, R.M. Hixon, Production of 2-Methylfuran by Vapor-Phase Hydrogenation of Furfural, Ind. Eng. Chem. 40 (1948) 502–505. https://doi.org/10.1021/ie50459a034.

[18] D.G. Manly, A.P. Dunlop, Catalytic Hydrogenation. I. Kinetics and Catalyst Composition in the Preparation of 2-Methylfuran, J. Org. Chem. 23 (1958) 1093–

1095. https://doi.org/10.1021/jo01102a002.

[19] D. Liu, D. Zemlyanov, T. Wu, R.J. Lobo-Lapidus, J.A. Dumesic, J.T. Miller, C.L. Marshall, Deactivation mechanistic studies of copper chromite catalyst for selective hydrogenation of 2-furfuraldehyde, J. Catal. 299 (2013) 336–345. https://doi.org/10.1016/j.jcat.2012.10.026.

[20] K. Yan, A. Chen, Efficient hydrogenation of biomass-derived furfural and levulinic acid on the facilely synthesized noble-metal-free Cu-Cr catalyst, Energy. 58 (2013) 357–363. https://doi.org/10.1016/j.energy.2013.05.035.

[21] F. Dong, Y. Zhu, H. Zheng, Y. Zhu, X. Li, Y. Li, Cr-free Cu-catalysts for the selective hydrogenation of biomass-derived furfural to 2-methylfuran: The synergistic effect of metal and acid sites, J. Mol. Catal. A Chem. 398 (2015) 140–148. https://doi.org/10.1016/j.molcata.2014.12.001.

[22] X. Yang, Q. Meng, G. Ding, Y. Wang, H. Chen, Y. lei Zhu, Y.W. Li, Construction of novel Cu/ZnO-Al_2O_3 composites for furfural hydrogenation: The role of Al components, Appl. Catal. A Gen. 561 (2018) 78–86. https://doi.org/10.1016/j.apcata.2018.04.005.

[23] X. Yang, X. Xiang, H. Chen, H. Zheng, Y.W. Li, Y. Zhu, Efficient Synthesis of Furfuryl Alcohol and 2-Methylfuran from Furfural over Mineral-Derived Cu/ZnO Catalysts, ChemCatChem. 9 (2017) 3023–3030. https://doi.org/10.1002/cctc.201700279.

[24] K.L. Deutsch, B.H. Shanks, Active species of copper chromite catalyst in C-O hydrogenolysis of 5-methylfurfuryl alcohol, J. Catal. 285 (2012) 235–241. https://doi.org/10.1016/j.jcat.2011.09.030.

[25] R. Rao, A. Dandekar, R.T.K. Baker, M.A. Vannice, Properties of Copper Chromite Catalysts in Hydrogenation Reactions, J. Catal. 171 (1997) 406–419.

https://doi.org/10.1006/jcat.1997.1832.

[26] R.S. Rao, R.T.K. Baker, M.A. Vannice, Furfural hydrogenation over carbon-supported copper, Catal. Letters. 60 (1999) 51–57. https://doi.org/10.1023/A:1019090520407.

[27] S. Sitthisa, W. An, D.E. Resasco, Selective conversion of furfural to methylfuran over silica-supported NiFe bimetallic catalysts, J. Catal. 284 (2011) 90–101. https://doi.org/10.1016/j.jcat.2011.09.005.

[28] M. Behrens, Meso- and nano-structuring of industrial Cu/ZnO/(Al_2O_3) catalysts, J. Catal. 267 (2009) 24–29. https://doi.org/10.1016/j.jcat.2009.07.009.

[29] S. Zander, E.L. Kunkes, M.E. Schuster, J. Schumann, G. Weinberg, D. Teschner, N. Jacobsen, R. Schlögl, M. Behrens, The role of the oxide component in the development of copper composite catalysts for methanol synthesis, Angew. Chemie - Int. Ed. 52 (2013) 6536–6540. https://doi.org/10.1002/anie.201301419.

[30] S. Mehta, G.W. Simmons, K. Klier, R.G. Herman, Catalytic synthesis of methanol from CO H2. II. Electron microscopy (TEM, STEM, microdiffraction, and energy dispersive analysis) of the Cu ZnO and Cu/ZnO/Cr2O3 catalysts, J. Catal. 57 (1979) 339–360. https://doi.org/10.1016/0021-9517(79)90001-0.

[31] R.B.C. Pillai, A study of the preactivation of a copper chromite catalyst, Catal. Letters. 26 (1994) 365–371. https://doi.org/10.1007/BF00810610.

[32] V.Z. Fridman, A.A. Davydov, A.A. Davydov, Dehydrogenation of cyclohexanol on copper-containing catalysts: I. The influence of the oxidation state of copper on the activity of copper sites, J. Catal. 195 (2000) 20–30. https://doi.org/10.1006/jcat.2000.2979.

[33] A.J.B.B. R. G. Herman, K. Klier, G. W. Simmons, B. P. Finn, Catalytic Synthesis of Methanol from CO / H , of oxygenated products from carbon mon-

ponents . The disadvantages of the Cu / significant :, J. Catal. 56 (1979) 407–429. https://doi.org/10.1016/0021-9517(79)90132-5.

[34] S. Mehta, G.W. Simmons, K. Klier, R.G. Herman, Catalytic synthesis of methanol from CO H_2. II. Electron microscopy (TEM, STEM, microdiffraction, and energy dispersive analysis) of the Cu ZnO and Cu/ZnO/Cr_2O_3 catalysts, J. Catal. 57 (1979) 339–360. https://doi.org/10.1016/0021-9517(79)90001-0.

[35] Y. Wang, J. Hao, G. Gong, R. Chen, Y. Su, Effects of atmosphere and Cu doping on the magnetic properties of ZnO powders, Phys. B Condens. Matter. 564 (2019) 22–27. https://doi.org/10.1016/j.physb.2019.04.005.

[36] M. Behrens, S. Zander, P. Kurr, N. Jacobsen, J. Senker, G. Koch, T. Ressler, R.W. Fischer, R. Schlögl, Performance improvement of nanocatalysts by promoter-induced defects in the support material: Methanol synthesis over Cu/ZnO:Al, J. Am. Chem. Soc. 135 (2013) 6061–6068. https://doi.org/10.1021/ja310456f.

[37] A.J.B.B. R. G. Herman, K. Klier, G. W. Simmons, B. P. Finn, Catalytic Synthesis of Methanol from CO / H , of oxygenated products from carbon mon-ponents . The disadvantages of the Cu / significant :, J. Catal. 56 (1979) 407–429. https://doi.org/http://dx.doi.org/10.1016/0021-9517(79)90132-5.

[38] S. Zheng, K. Zhu, W. Li, Y. Ji, Hydrogenation of dimethyl malonate to 1,3-propanediol catalyzed by a Cu/SiO_2 catalyst: The reaction network and the effect of Cu^+ /Cu^0 on selectivity, New J. Chem. 41 (2017) 5752–5763. https://doi.org/10.1039/c6nj03960j.

[39] W. Li, G. Fan, L. Yang, F. Li, Surface Lewis acid-promoted copper-based nanocatalysts for highly efficient and chemoselective hydrogenation of citral to unsaturated allylic alcohols, Catal. Sci. Technol. 6 (2016) 2337–2348.

https://doi.org/10.1039/c5cy01084e.

[40] A. Dandekar, R.T.K. Baker, M.A. Vannice, Carbon-Supported Copper Catalysts, J. Catal. 183 (1999) 131–154. https://doi.org/10.1006/jcat.1999.2390.

[41] P. Ai, M. Tan, Y. Ishikuro, Y. Hosoi, G. Yang, Y. Yoneyama, N. Tsubaki, Design of an Autoreduced Copper in Carbon Nanotube Catalyst to Realize the Precisely Selective Hydrogenation of Dimethyl Oxalate, ChemCatChem. 9 (2017) 1067–1075. https://doi.org/10.1002/cctc.201601503.

[42] Y. Zhao, S. Li, Y. Wang, B. Shan, J. Zhang, S. Wang, X. Ma, Efficient tuning of surface copper species of Cu/SiO_2 catalyst for hydrogenation of dimethyl oxalate to ethylene glycol, Chem. Eng. J. 313 (2017) 759–768. https://doi.org/10.1016/j.cej.2016.12.027.

[43] Y. Cui, B. Wang, C. Wen, X. Chen, W.L. Dai, Investigation of Activated-Carbon-Supported Copper Catalysts with Unique Catalytic Performance in the Hydrogenation of Dimethyl Oxalate to Methyl Glycolate, ChemCatChem. 8 (2016) 527–531. https://doi.org/10.1002/cctc.201501055.

[44] G.K. Williamson, W.H. Hall, X-ray line broadening from filed aluminium and wolfram, Acta Metall. 1 (1953) 22–31. https://doi.org/10.1016/0001-6160(53)90006-6.

[45] M.J. Campos Molina, R. Mariscal, M. Ojeda, M. López Granados, Cyclopentyl methyl ether: A green co-solvent for the selective dehydration of lignocellulosic pentoses to furfural, Bioresour. Technol. 126 (2012) 321–327. https://doi.org/10.1016/j.biortech.2012.09.049.

[46] X. Wang, K. Ma, L. Guo, Y. Tian, Q. Cheng, X. Bai, J. Huang, T. Ding, X. Li, Cu/ZnO/SiO 2 catalyst synthesized by reduction of ZnO-modified copper phyllosilicate for dimethyl ether steam reforming, Appl. Catal. A Gen. 540

(2017) 37–46. https://doi.org/10.1016/j.apcata.2017.04.013.

[47] J. Hu, Y. Song, J. Huang, Y. Li, M. Chen, H. Wan, New Insights into the Role of Al_2O_3 in the Promotion of CuZnAl Catalysts: A Model Study, Chem. - A Eur. J. 23 (2017) 10632–10637. https://doi.org/10.1002/chem.201701697.

[48] K.L. Deutsch, B.H. Shanks, Copper mixed metal oxide catalysts in the hydrogenolysis of 5-methylfurfuryl alcohol, Appl. Catal. A Gen. 470 (2014) 390–397. https://doi.org/10.1016/j.apcata.2013.11.020.

[49] J.R. Monnier, M.J. Hanrahan, G. Apai, A study of the catalytically active copper species in the synthesis of methanol over CuCr oxide, J. Catal. 92 (1985) 119–126. https://doi.org/10.1016/0021-9517(85)90241-6.

[50] W.M.R. C.D. Wagner, J.F. Moulder, L.E. Davis, Handbook of X-Ray Photoelectron Spectroscopy, 1992.

[51] S. Polarz, J. Strunk, V. Ischenko, M.W.E. Van Den Berg, O. Hinrichsen, M. Muhler, M. Driess, On the role of oxygen defects in the catalytic performance of zinc oxide, Angew. Chemie - Int. Ed. 45 (2006) 2965–2969. https://doi.org/10.1002/anie.200503068.

[52] S. Kattel, P.J. Ramírez, J.G. Chen, J.A. Rodriguez, P. Liu, Active sites for CO_2 hydrogenation to methanol on Cu/ZnO catalysts, Science (80-.). 355 (2017) 1296–1299. https://doi.org/10.1126/science.aal3573.

[53] C. Álvarez Galván, J. Schumann, M. Behrens, J.L.G. Fierro, R. Schlögl, E. Frei, Reverse water-gas shift reaction at the Cu/ZnO interface: Influence of the Cu/Zn ratio on structure-activity correlations, Appl. Catal. B Environ. 195 (2016) 104–111. https://doi.org/10.1016/j.apcatb.2016.05.007.

[54] M.B. Fichtl, J. Schumann, I. Kasatkin, N. Jacobsen, M. Behrens, R. Schlögl, M. Muhler, O. Hinrichsen, Counting of oxygen defects versus metal surface sites in

methanol synthesis catalysts by different probe molecules, Angew. Chemie - Int. Ed. 53 (2014) 7043–7047. https://doi.org/10.1002/anie.201400575.

[55] S. Kuld, C. Conradsen, P.G. Moses, I. Chorkendorff, J. Sehested, Quantification of zinc atoms in a surface alloy on copper in an industrial-type methanol synthesis catalyst, Angew. Chemie - Int. Ed. 53 (2014) 5941–5945. https://doi.org/10.1002/anie.201311073.

[56] M. Behrens, F. Studt, I. Kasatkin, S. Kühl, M. Hävecker, F. Abild-Pedersen, S. Zander, F. Girgsdies, P. Kurr, B.L. Kniep, M. Tovar, R.W. Fischer, J.K. Nørskov, R. Schlögl, The active site of methanol synthesis over $Cu/ZnO/Al_2O_3$ industrial catalysts, Science (80-.). 336 (2012) 893–897. https://doi.org/10.1126/science.1219831.

[57] X. Yang, H. Chen, Q. Meng, H. Zheng, Y. Zhu, Y.W. Li, Insights into influence of nanoparticle size and metal-support interactions of Cu/ZnO catalysts on activity for furfural hydrogenation, Catal. Sci. Technol. 7 (2017) 5625–5634. https://doi.org/10.1039/c7cy01284e.

[58] M. Thommes, K. Kaneko, A. V. Neimark, J.P. Olivier, F. Rodriguez-Reinoso, J. Rouquerol, K.S.W. Sing, Physisorption of gases, with special reference to the evaluation of surface area and pore size distribution (IUPAC Technical Report), Pure Appl. Chem. 87 (2015) 1051–1069. https://doi.org/10.1515/pac-2014-1117.

[59] J. Landers, G.Y. Gor, A. V. Neimark, Density functional theory methods for characterization of porous materials, Colloids Surfaces A Physicochem. Eng. Asp. 437 (2013) 3–32. https://doi.org/10.1016/j.colsurfa.2013.01.007.

[60] G.R. Bertolini, C.P. Jiménez-Gómez, J.A. Cecilia, P. Maireles-Torres, Gas-Phase Hydrogenation of Furfural to Furfuryl Alcohol over $Cu\text{-}ZnO\text{-}Al_2O_3$ Catalysts Prepared from Layered Double Hydroxides, Catalysts. 10 (2020) 486.

https://doi.org/10.1201/9780429022944-22.

[61] J. Gong, H. Yue, Y. Zhao, S. Zhao, L. Zhao, J. Lv, S. Wang, X. Ma, Synthesis of ethanol via syngas on Cu/SiO_2 catalysts with balanced Cu^0 -Cu^+ sites, J. Am. Chem. Soc. 134 (2012) 13922–13925. https://doi.org/10.1021/ja3034153.

[62] Y. Liu, Y. Liu, H. Wang, J. Zhao, C. Liu, Reactive Adsorption Desulfurization on Cu/ZnO Adsorbent: Effect of ZnO Polarity Ratio on Selective Hydrogenation, Energy and Fuels. 31 (2017) 9930–9938. https://doi.org/10.1021/acs.energyfuels.7b01935.

[63] I. Eswaramoorthi, V. Sundaramurthy, A.K. Dalai, Partial oxidation of methanol for hydrogen production over carbon nanotubes supported Cu-Zn catalysts, Appl. Catal. A Gen. 313 (2006) 22–34. https://doi.org/10.1016/j.apcata.2006.06.052.

[64] V.G. Ilves, M.G. Zuev, A.M. Murzakaev, S.Y. Sokovnin, Investigation of structural, magnetic and luminescent properties of weakly-doped ZnO–Cu nanopowders, produced by the pulsed electron beam evaporation, Mater. Chem. Phys. 225 (2019) 200–212. https://doi.org/10.1016/j.matchemphys.2018.12.069.

[65] P.P. Bui, S.T. Oyama, A. Takagaki, B.P. Carrow, K. Nozaki, Reactions of 2-Methyltetrahydropyran on Silica-Supported Nickel Phosphide in Comparison with 2-Methyltetrahydrofuran, ACS Catal. 6 (2016) 4549–4558. https://doi.org/10.1021/acscatal.6b01033.

[66] A. Infantes-Molina, E. Gralberg, J.A. Cecilia, E. Finocchio, E. Rodríguez-Castellón, Nickel and cobalt phosphides as effective catalysts for oxygen removal of dibenzofuran: Role of contact time, hydrogen pressure and hydrogen/feed molar ratio, Catal. Sci. Technol. 5 (2015) 3403–3415. https://doi.org/10.1039/c5cy00282f.

[67] M. Kurtz, J. Strunk, O. Hinrichsen, M. Muhler, K. Fink, B. Meyer, C. Wöll,

Active sites on oxide surfaces: ZnO-catalyzed synthesis of methanol from CO and H_2, Angew. Chemie - Int. Ed. 44 (2005) 2790–2794. https://doi.org/10.1002/anie.200462374.

[68] Y. Huang, W. Zhang, Z. Yue, X. Zhao, Z. Cheng, Performance of SiO_2–TiO_2 Binary Oxides Supported Cu–ZnO Catalyst in Ethyl Acetate Hydrogenation to Ethanol, Catal. Letters. 147 (2017) 2817–2825. https://doi.org/10.1007/s10562-017-2165-7.

[69] H. Zhang, Y. Lei, A.J. Kropf, G. Zhang, J.W. Elam, J.T. Miller, F. Sollberger, F. Ribeiro, M.C. Akatay, E.A. Stach, J.A. Dumesic, C.L. Marshall, Enhancing the stability of copper chromite catalysts for the selective hydrogenation of furfural using ALD overcoating, J. Catal. 317 (2014) 284–292. https://doi.org/10.1016/j.jcat.2014.07.007.

[70] H. Liu, Q. Hu, G. Fan, L. Yang, F. Li, Surface synergistic effect in well-dispersed Cu/MgO catalysts for highly efficient vapor-phase hydrogenation of carbonyl compounds, Catal. Sci. Technol. 5 (2015) 3960–3969. https://doi.org/10.1039/c5cy00437c.

[71] M. Ghashghaee, S. Shirvani, M. Ghambarian, Kinetic models for hydroconversion of furfural over the ecofriendly Cu-MgO catalyst: An experimental and theoretical study, Appl. Catal. A Gen. 545 (2017) 134–147. https://doi.org/10.1016/j.apcata.2017.07.040.